Linked halokinesis and mud volcanism at the Mercator mud volcano, Gulf of Cadiz

Carolina Perez-Garcia,[1] Christian Berndt,[2,3] Dirk Klaeschen,[2] Jürgen Mienert,[1] Laura Haffert,[2] Davy Depreiter,[4] and Matthias Haeckel[2]

Received 25 October 2010; revised 6 February 2011; accepted 14 February 2011; published 19 May 2011.

[1] Mud volcanoes are seafloor expressions of focused fluid flow that are common in compressional tectonic settings. New high-resolution 3-D seismic data from the Mercator mud volcano (MMV) and an adjacent buried mud volcano (BMV) image the internal structure of the top 800 m of sediment at both mud volcanoes, revealing that both are linked and have been active episodically. The total volumes of extruded mud range between 0.15 and 0.35 km^3 and 0.02–0.05 km^3 for the MMV and the BMV, respectively. The pore water composition of surface sediment samples suggests that halokinesis has played an important role in the evolution of the mud volcanoes. We propose that erosion of the top of the Vernadsky Ridge that underlies the mud volcanoes activated salt movement, triggering deep migration of fluids, dissolution of salt, and sediment liquefaction and mobilization since the end of the Pliocene. Since beginning of mud volcanism in this area, the mud volcanoes erupted four times while there was only one reactivation of salt tectonics. This implies that there are other mechanisms that trigger mud eruptions. The stratigraphic relationship of mudflows from the MMV and BMV indicates that the BMV was triggered by the MMV eruptions. This may either be caused by loading-induced hydrofracturing within the BMV or due to a common feeder system for both mud volcanoes. This study shows that the mud volcanoes in the El Arraiche mud volcano field are long-lived features that erupt with intervals of several tens of thousands of years.

Citation: Perez-Garcia, C., C. Berndt, D. Klaeschen, J. Mienert, L. Haffert, D. Depreiter, and M. Haeckel (2011), Linked halokinesis and mud volcanism at the Mercator mud volcano, Gulf of Cadiz, *J. Geophys. Res.*, *116*, B05101, doi:10.1029/2010JB008061.

1. Introduction

[2] Mud volcanoes and cold seeps in general have been an important target for the Hot spots Ecosystem Research on the Margins of European Seas (HERMES) project due to their control on deep sea biota and on carbon and sulphur turnovers at the European margins [*Foucher et al.*, 2009]. A challenging issue for the HERMES community has been to understand the temporal variability of fluid flow activity at such seep sites. Understanding these systems is also important for quantifying their contribution to the global biogeochemical carbon cycle. So far, understanding of marine mud volcanoes has been largely hampered by insufficient seismic imaging capabilities and ill-constrained eruption histories. Thus, feeder system processes had to be inferred from drilling (e.g., IODP Leg 160) or surface cores. Here, we present the first high-resolution 3-D seismic data for mud volcanoes in the Gulf of Cadiz.

[3] The Mercator mud volcano (MMV) and buried mud volcano (BMV) can be found in the El Arraiche mud volcano field which is the most recently discovered cluster of submarine mud volcanoes in the Gulf of Cadiz [*Van Rensbergen et al.*, 2003] increasing the number of known mud volcanoes in the area to more than thirty [*Gardner*, 2001]. The mud volcanoes in the El Arraiche field are similar in shape and size to other mud volcanoes in the Gulf of Cadiz [*Fernandez-Puga et al.*, 2007; *Somoza et al.*, 2003; *Van Rensbergen et al.*, 2005a] and appear as stacked mudflow edifices, i.e., the typical "Christmas tree" structures, on reflection seismic cross sections. Geochemical data indicate deeply rooted fluid sources below both the MMV and a BMV [*Hensen et al.*, 2007; *Scholz et al.*, 2009].

[4] The objectives of this study are to calculate the mud discharge rate and diameter of feeder conduits for both the MMV and BMV, to constrain the type and the magnitude of the eruptions of the MMV and the BMV, and to understand what controls these parameters. Furthermore, we investigate

[1]Department of Geology, University of Tromsø, Tromsø, Norway.
[2]IFM-GEOMAR, Leibniz Institute of Marine Sciences, Kiel University, Kiel, Germany.
[3]National Oceanography Centre, Southampton, UK.
[4]Renard Centre of Marine Geology, Department of Geology and Soil Science, Ghent University, Gent, Belgium.

0148-0227/11/2010JB008061

in which ways salt tectonics have affected the mud volcanism and how the closely spaced mud volcanoes are linked.

2. Geological Setting

[5] The Gulf of Cadiz is located at the compressional plate boundary between Eurasia and Africa (Figure 1a). Compression since the Late Tortonian led to the development of a thrust belt that covers the eastern part of the Gulf of Cadiz [e.g., *Maldonado et al.*, 1999; *Somoza et al.*, 1999], which is variably called the accretionary prism, olistostrome, or allochtonous unit of the Gulf of Cadiz (AUGC). It consists of a succession of Triassic (Atlantic synrift) [*Tari et al.*, 2000], Cretaceous, Paleogene and Neogene sedimentary units in different provinces, overlying Paleozoic basement [*Maldonado et al.*, 1999]. Thrusting of thick Mesozoic nappes in the distal part of the Gibraltar Arc resulted in large volumes of Triassic salt (mainly gypsum) being emplaced over younger strata [*Berástegui et al.*, 1998; *Maestro et al.*, 2003] forming salt allochthons. The last episode of active compression lasted at least from mid-Oligocene up to late Miocene times and is possibly still ongoing [e.g., *Rosenbaum et al.*, 2002; *Vázquez and Vegas*, 2000].

[6] Northwest Morocco's arcuate fold and thrust belts extend some 450 km offshore west into the southern Gulf of Cadiz [*Flinch*, 1993]. Offshore the city of Larrache (Figure 1a), folds and thrusts are cut by NW-SE trending normal faults [*Flinch*, 1993]. Here, the El Arraiche mud volcano field is located within the accretionary wedge of the Gulf of Cadiz but outside of the main AUGC [*Van Rensbergen et al.*, 2005a] (Figures 1a and 1b). The crests of the two main NW-SE striking anticlines that bound the group of mud volcanoes, i.e., Renard and Vernadsky ridges (Figure 1b), are offset by two NE-SW striking deformation zones [*Van Rensbergen et al.*, 2005a] related to strike-slip faulting [*Medialdea et al.*, 2009; *Van Rensbergen et al.*, 2005a].

[7] *Van Rensbergen et al.* [2005a] correlated the regional seismic reflectors in the El Arraiche field to the industry well LAR-1. They dated the base of the mud volcanoes to the Upper Pliocene unconformity and assigned an age of 2.4 Ma. After *Mascarelli* [2009], the base Quaternary has been reassigned from 1.8 Ma to 2.6 Ma, now fitting with the Upper Pliocene unconformity (UPR). Successive extrusion of mud from the cluster of mud volcanoes created vertical successions of mud edifices or Christmas tree structures up to 500 m thick, similar to other mud volcanoes in the Gulf of Cadiz [*Somoza et al.*, 2003]. The MMV is located in an L-shaped graben on top of Vernadsky Ridge (Figure 1b). The MMV is asymmetric with a moat along its southwestern side. It rises approximately 140 m above the surrounding seabed and has a maximum diameter of 245 m. The mudflows at the surface are semiconcentric [*Van Rensbergen et al.*, 2005a]. A crater and a 38 m high central dome top the mud volcano. A small BMV south of the MMV also occurs inside the L-shaped graben [*Van Rensbergen et al.*, 2005a, 2005b].

[8] Clay mineral dehydration during the transformation of smectite to illite is one of the most common sources of fluids that drive mud volcanoes worldwide, and many mud volcanoes in the Gulf of Cadiz are fuelled by this kind of fluid source [*Pinheiro et al.*, 2003; *Hensen et al.*, 2007]. *Hensen et al.* [2007] showed that halite dissolution occurs at other mud volcanoes in the Gulf of Cadiz (i.e., Captain Arutjunov MV).

3. Data and Method

[9] The high-resolution P cable 3-D seismic system was developed in a joint project between Volcanic Basin Petroleum Research (Oslo, Norway), the National Oceanography Centre (Southampton, UK), the University of Tromsø (Tromsø, Norway), and IFM-GEOMAR (Kiel, Germany) [*Planke and Berndt*, 2002; *Petersen et al.*, 2010]. A wire is towed perpendicular to the ship's steaming direction by two paravanes. In our experiment eleven analog single-channel streamers were connected to this wire. The seismic source consisted of an array of four 40 in^3 Bolt 600B air guns with a frequency range from 30 to 350 Hz, centered around 120 Hz. Unintended firing of a 5th gun resulted in coherent noise approximately 250 ms below the seafloor (Figures 4, 6, and 7). The analog signal was recorded with a Geometrix Geode 24 recording system. The seismic data are positioned using a Kongsberg DGPS system consisting of two DGPS antennae on the paravanes, one on the gun float and one onboard.

[10] The 3-D high-resolution seismic data set collected during the RRS *Charles Darwin* cruise 178 (March-April 2006) covers an area of 9.95 km × 3.2 km, composed of 56 sail lines with a shot point interval of approximately 12.5 m. The processing included navigation corrections, filtering, and image processing. To ensure that the navigation is consistent with the observed arrival times of the direct wave, all arrival times of the direct wave on every channel were picked automatically. From the arrival times of the two outermost channels close to the paravanes a relocated shot position was calculated. By assuming a triangular shape as a starting geometry of the cross cable, each channel was repositioned along the sail line direction to match the direct wave arrival time. To enable a consistent depth of the subsurface structure imaged by different loops of the sail lines, a shot date-depending tidal correction was applied. Besides editing, band-pass filtering, and scaling seismic processing included a short gap predictive deconvolution to remove the receiver ghost due to varying depths of the streamers. To image the shallow complex structures a true amplitude 3-D prestack time migration with a bin size of 10 m × 10 m resulted in the best signal-to-noise ratio. The migration was limited to frequencies up to 220 Hz to avoid spatial aliasing. Thus, the maximum vertical resolution of the data is approximately 3–4 m (as centered in 120 Hz) and the maximum horizontal resolution approximately 10–15 m, both decreasing downward.

[11] The migration results, i.e., the small number of remaining diffraction hyperbolae, show that a velocity depth function of 1500 m/s for the water column and 1900 m/s for the first 1 s of seismic data are a suitable approximation for conducting the time depth conversion of the 3-D seismic data set. These values for the P wave velocity are consistent with the first P wave interval velocities estimated by *Depreiter* [2009] for the area close to the Pen Duick escarpment, in the El Arraiche field. Due to free gas the velocities may vary by up to 50% locally within the mud volcanoes, but the time depth conversion should be accurate to +/− 20% within the mud volcano and +/− 5–10% for the sediments in the sediments surrounding the mud volcanoes.

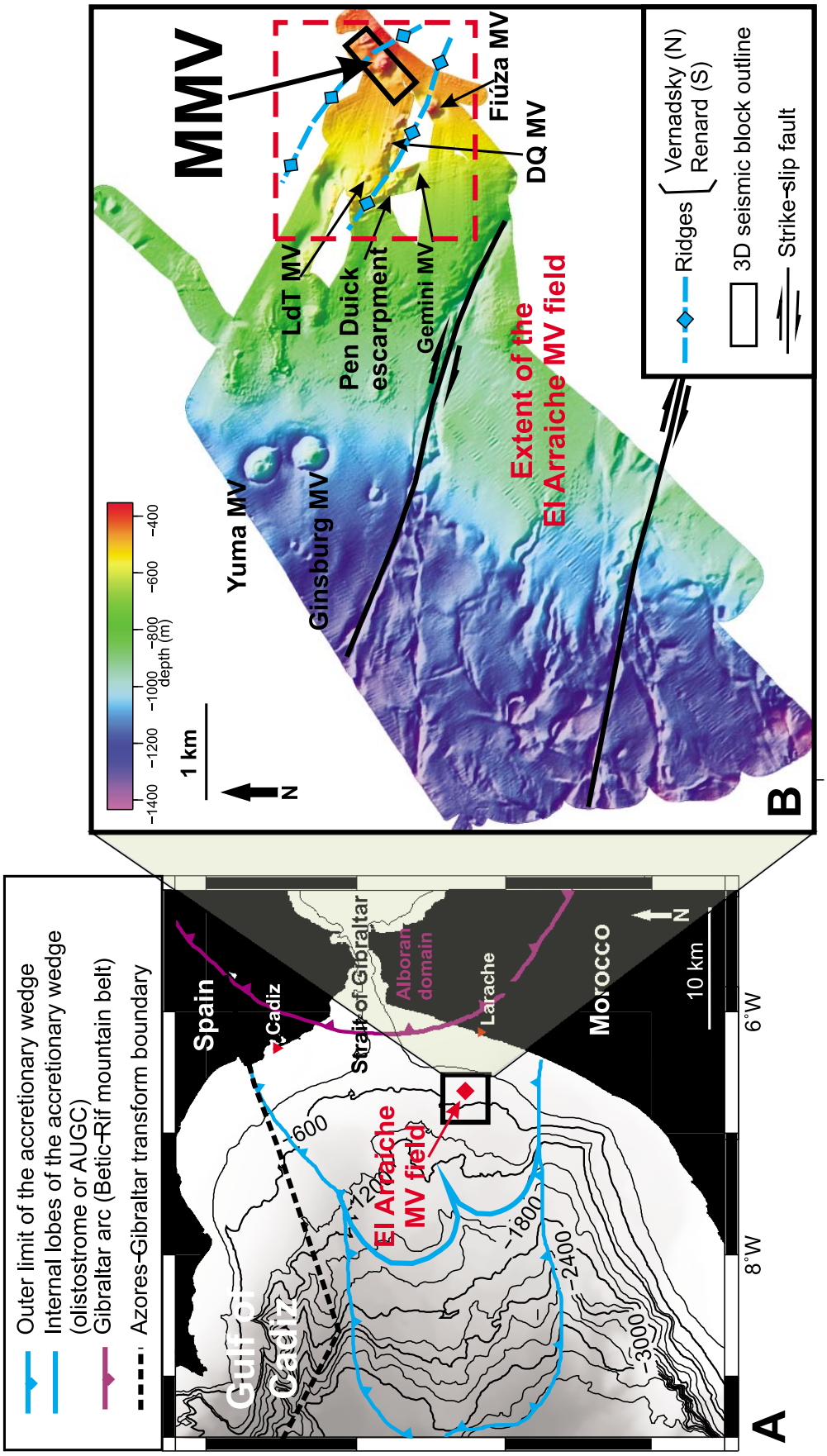

Figure 1. (a) Location map of the El Arraiche mud volcano field and the Mercator mud volcano (MMV) in the Gulf of Cadiz. The bathymetry data is based on *Sandwell and Smith* [1997]. The outer limit of the accretionary wedge, its internal lobes, the Azores-Gibraltar transform, and the Gibraltar Arc are based on *Gutscher et al.* [2009] and *Medialdea et al.* [2009]. (b) Multibeam swath bathymetry of the continental shelf and upper slope at NW Morocco; red dotted square, extension of the El Arraiche mud volcano field; black square, outer limit of the 3-D seismic data set over the Vernadsky Ridge; LdT, Lazarillo de Tormes MV; DQ, Don Quichote MV.

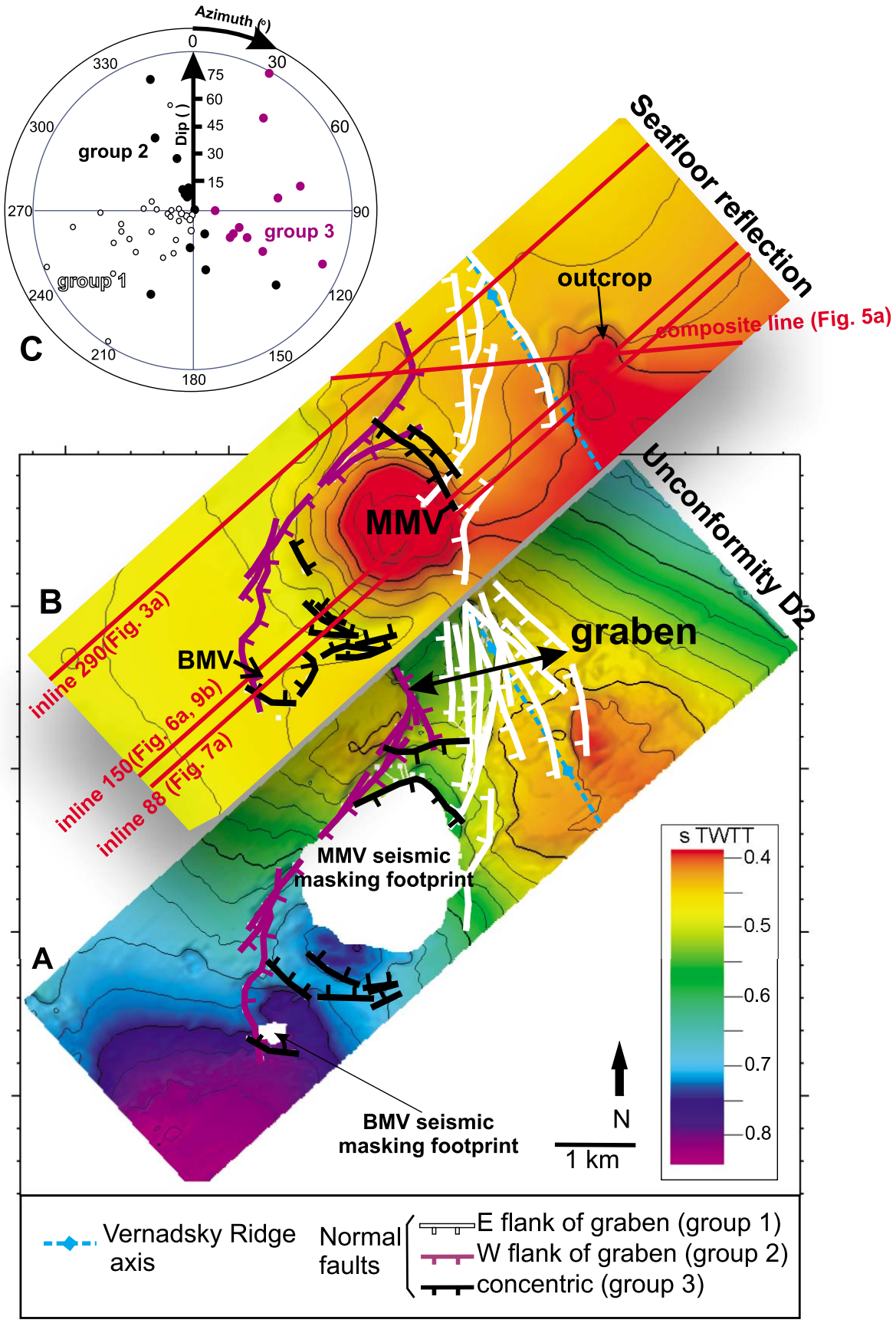
Azimuth (°)
0
30
60
90
120
150
180
210
240
270
300
330
Dip (°)
75
60
45
30
15
group 2
group 3
group 1
C
Seafloor reflection
outcrop
composite line (Fig. 5a)
Unconformity D2
MMV
B
graben
BMV
inline 290(Fig. 3a)
inline 150(Fig. 6a, 9b)
inline 88 (Fig. 7a)
MMV seismic masking footprint
A
BMV seismic masking footprint
N
1 km
s TWTT
0.4
0.5
0.6
0.7
0.8
Vernadsky Ridge axis
Normal faults
E flank of graben (group 1)
W flank of graben (group 2)
concentric (group 3)

Figure 2

[12] Different modules of Petrel 2008.1 (Schlumberger) have been used to perform seismic interpretation of both horizons and faults and to estimate both dip of reflections and total volume of mud extruded from the mud volcanoes. The "ant-tracking" module uses a workflow of seismic attributes to identify and track faults through preprocessed 3-D seismic volumes [*Pedersen et al.*, 2002] based on the detection of correlated interruptions in the amplitude of the seismic cube. The ant-tracking workflow includes edge detection and edge enhancing [*Pedersen et al.*, 2005] which localizes and emphasizes the edge of the amplitude discontinuities. The result is an attribute volume that is optimized for structural interpretation using the fault extraction module (Figure 2) and manages the display of the internal structure of the mud volcanoes. In addition, we use the "variance (edge method)" attribute [*van Bemmel and Pepper*, 2000]. The variance attribute measures the deviations from the mean value of amplitude and is used to isolate discontinuities in the horizontal continuity (edges) from the input seismic cube. Three parameters, i.e., inline and cross-line number of traces to include in the calculation and vertical smoothing, control the variance attribute. The vertical smoothing parameter diminishes residual horizontal structures and improves the imaging of vertical events. We use values of three traces for both the inline and the cross-line range, and a vertical smoothing of 0.01 s. The "local structural dip" attribute (Figure 3c) describes the angle of inclination of each seismic event as measured from a horizontal plane (0 to 90 degrees) with the normal positive upward. The gradient is computed in both the inline and cross-line directions to create a 3-D gradient function. This is a suitable attribute to define volumes of same dip. For the estimation of the mud volumes extruded from the mud volcanoes we generated geobodies for the original 3-D seismic data set to isolate connected values of amplitude that surpass a threshold determined by tests. The chaotic signature that represents the mud extrusions can be easily isolated from the surrounding hemipelagic sediments using a graphic equalizer, structural smoothing and chaos volume attributes. Minimum and maximum values of volume of mud for each mud volcano are qualitatively related to the gas (methane) content within the mud breccias. We used velocity values of 1500 ms^{-1} and 1900 ms^{-1} (based on seismic velocity analyses of multichannel seismic data) [*Depreiter*, 2009] related to very high and very low methane content within the mud breccias, corresponding to the minimum and maximum volume of mud extracted, respectively.

[13] The bathymetry of the El Arraiche field (Figure 1b) is based on the hull mounted SIMRAD EM12 system and was collected during the same cruise. It was processed using Kongsberg's Neptune software and gridded at 50 × 50 m using Generic Mapping Tools [*Wessel and Smith*, 1998] and integrated into the seismic interpretation project.

[14] Additionally, geochemical data were collected during the expedition MSM 1/3 in 2006 with R/V Maria S. Merian. We sampled surface sediments from the top of the MMV using a gravity corer (GC). The maximum sediment retriever was 2 m. Subsamples were taken for geochemical analyses of dissolved pore water constituents (e.g., anions, cations, gases). Pore water was extracted from the wet sediment with a low-pressure (Ar at 1–5 bar) filtration system and aliquots were analyzed for dissolved sodium and chloride concentrations by ICP-AES (inductively coupled plasma atomic emission spectroscopy) and IC (ion chromatography), respectively. A detailed description of sampling procedures and analytical methods is given by *Scholz et al.* [2009].

4. Results

4.1. Structural Analysis

[15] The structural analysis of the seismic data set shows three main groups of normal fault azimuth directions, i.e., SW (group 1), NE (group 2) and N and S (group 3) (Figures 2a–2c). Groups 1 and 2 correspond to the eastern and western flanks of a local L-shaped graben, respectively. Group 3 includes the major concentric normal faults around the MMV (Figures 2a–2c). In general, the normal faults dip steeply and those forming the flanks of the graben reach all the way up to the seafloor (Figures 2a and 2b). An NE-SW oriented seismic line (Figures 3a–3c) shows that the crest of the Vernadsky Ridge (Figure 1b) partially collapses into the L-shaped graben as it strikes NW-SE and N-S (Figure 4).

[16] Figure 3c shows the dip of reflections of a typical inline (inline 290, Figure 3a) measured from a horizontal plane in degrees, i.e., local structural dip as described in section 3. We observe three main reflector dip groups, i.e., steep, intermediate, and flat dip groups (Figures 3c and 3d). These groups are separated by the two major unconformities (truncations) that can be identified in the study area: D2 (between the steep and the intermediate dip group, Figure 3b) and D1 (between the intermediate and the flat dip group) (Figures 3a and 3b, respectively). Considering each dip group a tectonofacies we call them Tf3 (steep), Tf2 (intermediate) and Tf1 (flat) from deep to shallow (Figure 3d).

[17] An E-W oriented composite line across the graben (Figures 5a and 5b) reveals abrupt termination of internal reflections in the hanging wall of a normal fault that forms its eastern flank. This flank is tilted up and crops out at the seafloor (Figures 2a, 5a, and 5b). An antithetic normal fault constitutes the western flank of the graben (Figures 5a and 5b).

4.2. Mud Volcanoes

4.2.1. Mud Volcano Seismic Signature and Internal Structure

[18] Internal reflections within each tectonofacies are laterally continuous and stratified, except for unconformities D1 and D2 (e.g., Figure 3a) and some local interruptions by the chaotic seismic signature of the mud volcanoes (Figure 6a). The flanks of the L-shaped graben limit the extension of the

Figure 2. General structural map of the study area. (a) Main failure below the unconformity D2. Normal faults forming the eastern and western flanks of the graben strongly affect D2. The circular areas of no interpretation correspond to the chaotic signature of the mud volcano edifices across D2. (b) Still active faults above the seafloor reflection. Note that both MMV and a buried mud volcano (BMV) are located in the graben on the crest of the Vernadsky Ridge. (c) Rose diagram of the main failure trends, showing the azimuth and dip values of the main faults described in Figures 2a and 2b, classified in group 1 (eastern flank of the graben), group 2 (western flank of the graben), and group 3 (concentric faults).

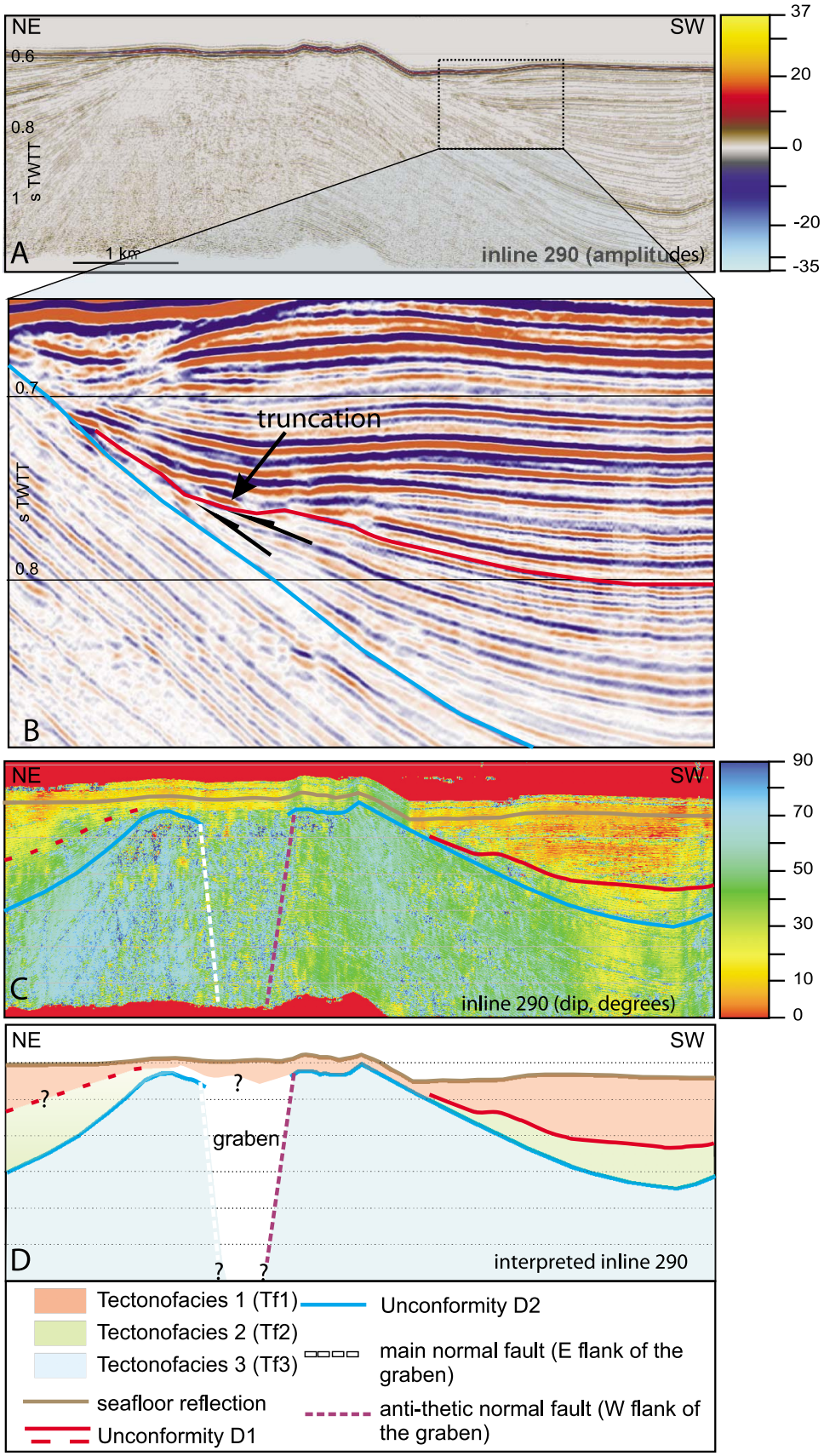
NE
SW
0.6
0.8
1
s TWTT
A
1 km
inline 290 (amplitudes)
37
20
0
-20
-35
0.7
truncation
s TWTT
0.8
B
NE
SW
C
inline 290 (dip, degrees)
90
70
50
30
10
0
NE
SW
?
?
graben
?
?
D
interpreted inline 290
Tectonofacies 1 (Tf1)
Tectonofacies 2 (Tf2)
Tectonofacies 3 (Tf3)
seafloor reflection
Unconformity D1
Unconformity D2
main normal fault (E flank of the graben)
anti-thetic normal fault (W flank of the graben)

Figure 3

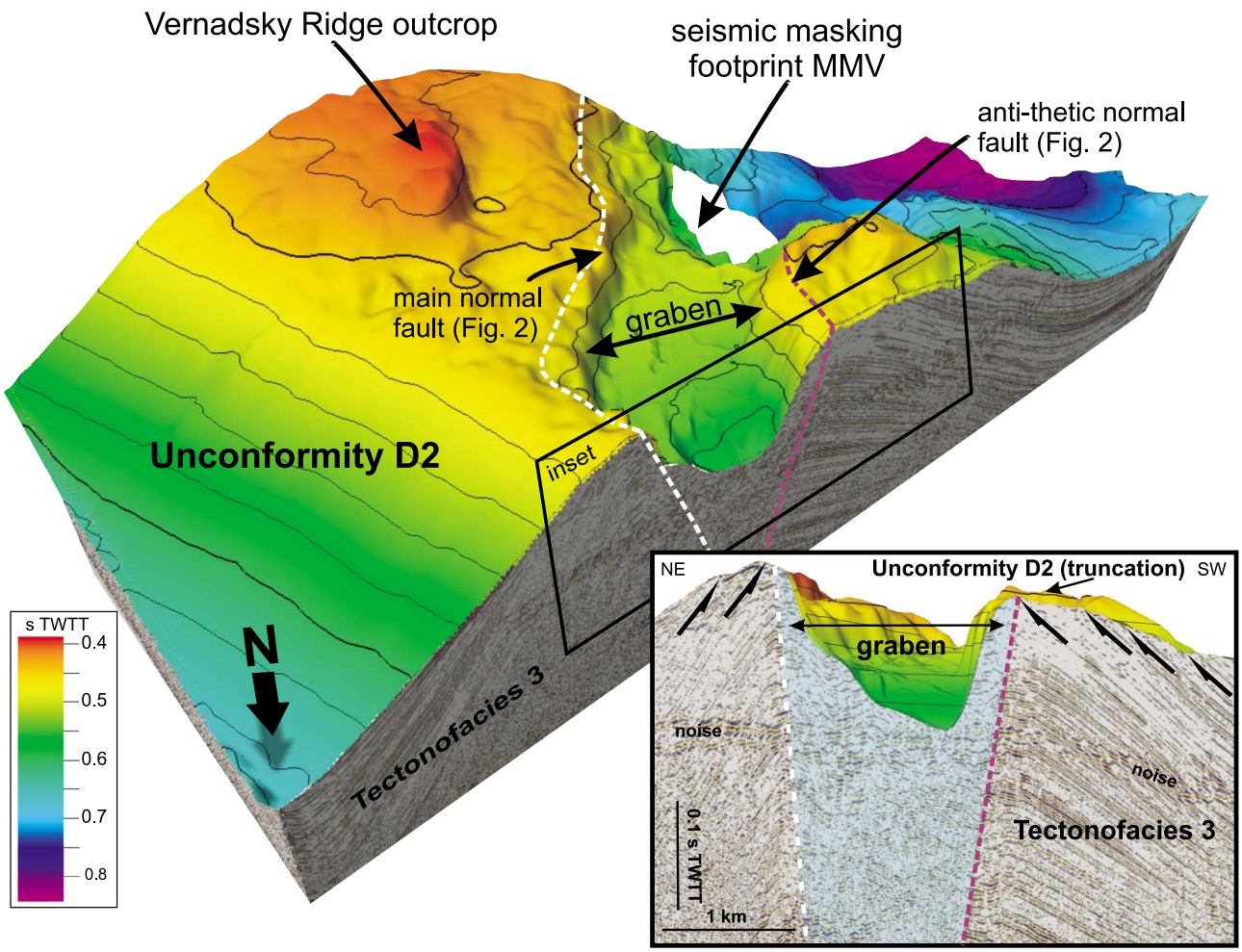

Figure 4. Three-dimensional view of the 3-D seismic data set from the north at the time of the D2 erosion. Note the L-shaped graben and the location of the chaotic signature of the MMV. The eastern flank of the graben tilts upward and crops out at the seafloor. Inset shows detail of D2 truncation at the top of Vernadsky Ridge.

chaotic seismic signature of both MMV and BMV (Figures 4 and 6a). The top 0.5 s two-way travel time (TWT) of the MMV and the top 0.3 s TWT of the BMV (i.e., measured from the seafloor reflection) consist of a succession of sediment units that protrude from concentric disturbance zones of ~2 km and ~0.6 km maximum diameter, respectively, and interfinger with the surrounding layered sediments (Figure 6a). These protrusions are commonly called Christmas tree structures and interpreted as mudflow units deposited during active phases of a mud volcano and subsequently buried by nonmud/nonvolcanic sediments during long periods of quiescence [e.g., *Hovland and Judd*, 1988; *Kopf*, 2002; *Somoza et al.*, 2003; *Calvès et al.*, 2010]. Following this interpretation the depth intervals with protrusions represent the extrusive parts of the mud volcano (i.e., mudflows), and the stratigraphic level of the lowermost mudflows indicates the base of the mud volcano initiation. The base reflection of the extrusive part of both MMV and BMV is the unconformity D1 (Figures 5 and 6a).

[19] Figure 7 shows time slices through the ant-tracking cube (Figure 7b) and the variance cube (7c) of five different time events across both the MMV and the BMV mud edifices (Figure 7a). The ant-tracking derived discontinuities, i.e., joined-up areas with low seismic reflection amplitude, are not randomly distributed in the center of the mud edifices. They can be followed across several of the time slices and are concentric toward the edges of the MMV feeder system. The variance attribute shows a more random pattern for the MMV and strong horizontal variability in the BMV. The lateral variability and horizontal continuity of these attributes indicates that the internal structure of the feeder system is heterogeneous. Although some of these seismic anomalies may be the result of imperfect imaging (e.g., the effects of

Figure 3. Local structural dip and main tectonofacies: (a) the 3-D seismic inline 290 (see location in Figure 2b) shows the collapsed graben at the crest of the Vernadsky Ridge and its top truncation by unconformity D2 (blue line), (b) detail of the truncation by unconformity D1 (red line), (c) the qualitative classification of different degrees of dipping reveals three groups or tectonofacies, and (d) interpreted inline 290, showing the three tectonofacies separated by the main unconformities.

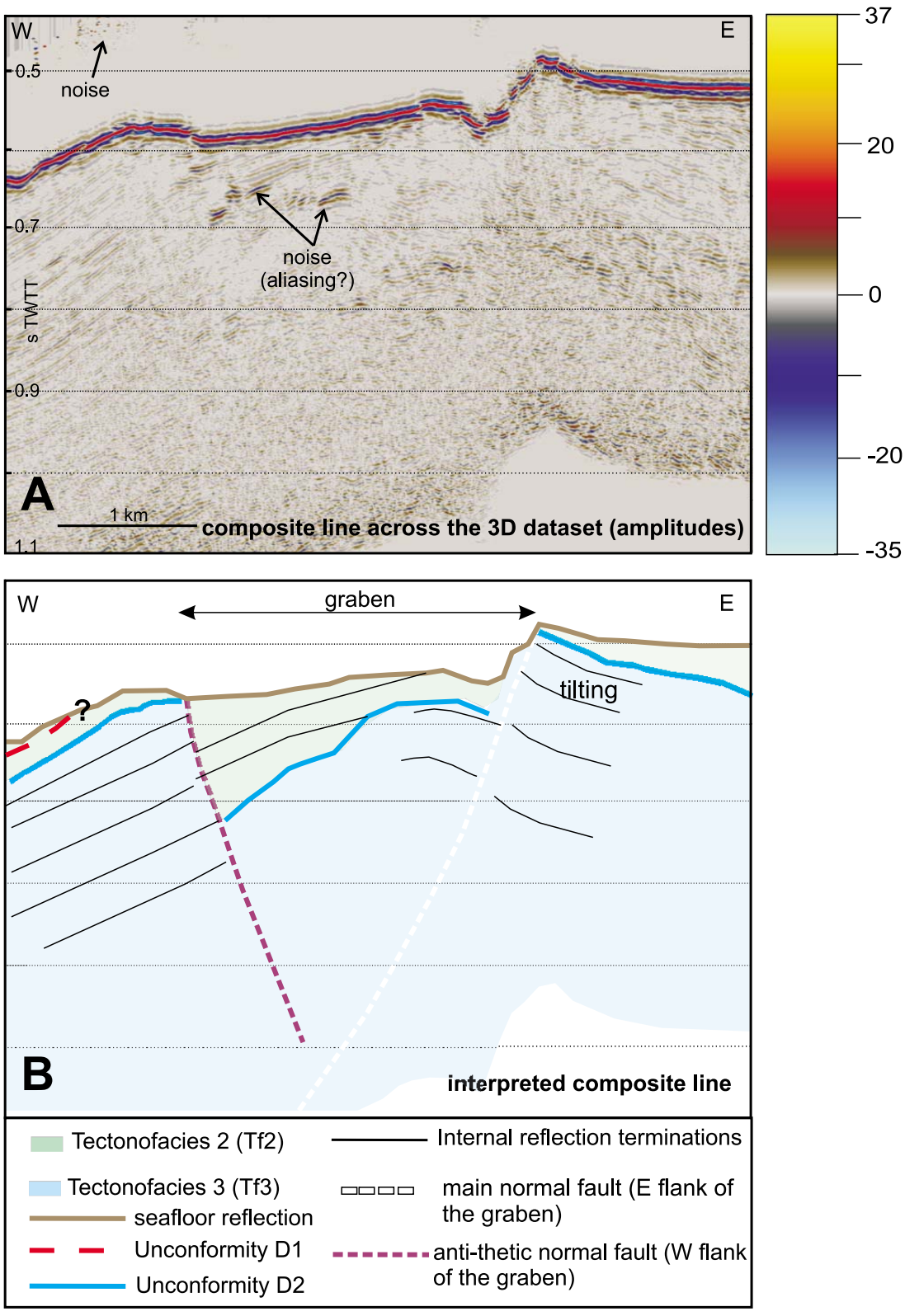

Figure 5. (a) Composite seismic line across the graben, extracted from the 3-D seismic block. Note the tilting of the eastern flank of the graben and the antithetic normal fault of the western flank of the graben (see location in Figure 2b). (b) Interpreted composite line showing the distribution of tectonofacies.

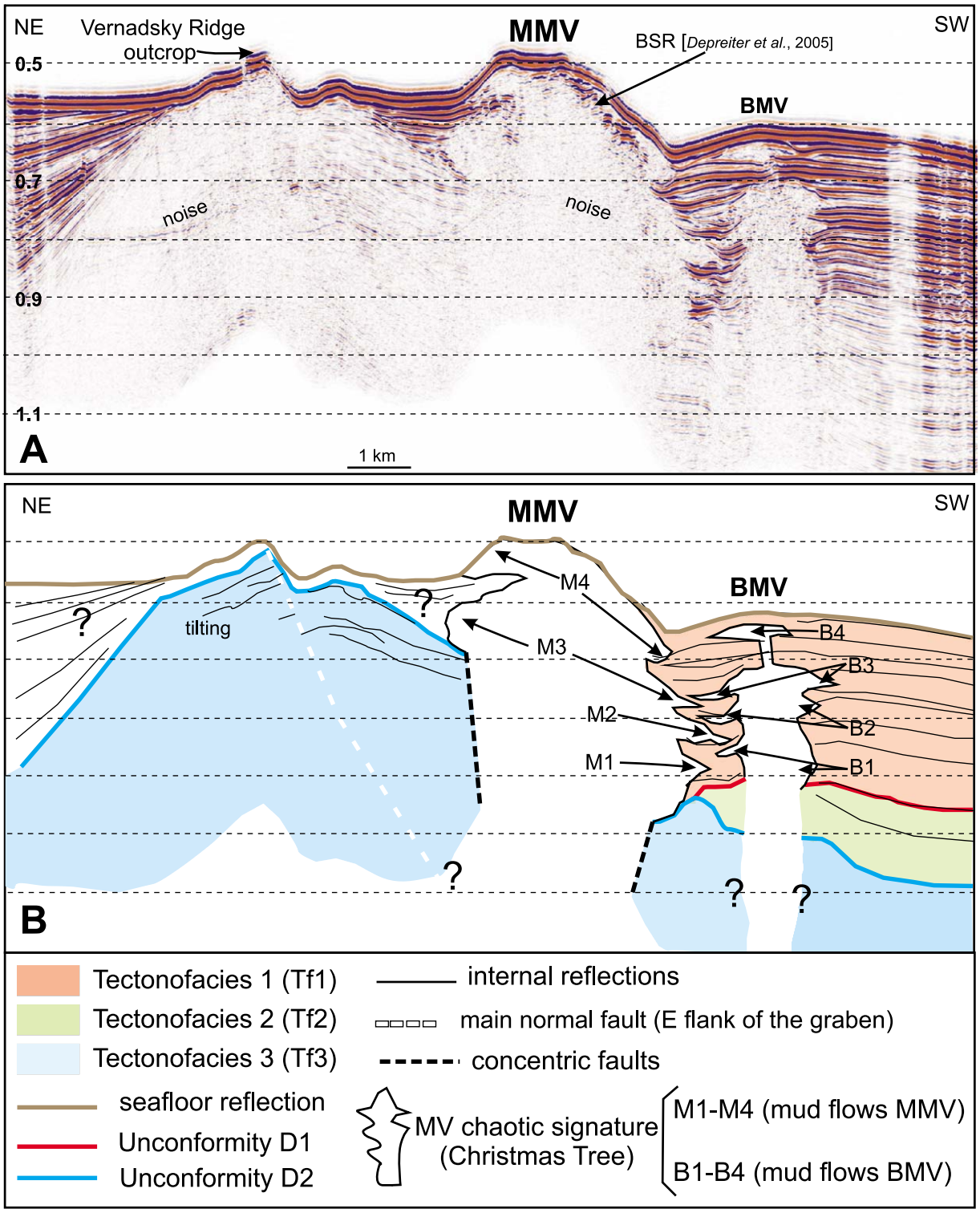

Figure 6. Mud volcano seismic signature: (a) inline across both MMV and BMV, extracted from the 3-D seismic block; bottom simulating reflector (BSR) described by *Depreiter et al.* [2005] and (b) interpreted seismic inline showing the tectonofacies distribution and the interfingering of mud extrusions with tectonofacies 1 (Tf1).

diffracted energy or tuning effects), the consistency of the seismic facies distribution and its repetitive pattern in time slices suggests that the seismic data can indeed be used to describe the nature of the feeder system. Ant-tracking and variances time slices are also used to resolve the feeder system of the Caspian Sea mud volcanoes and salt domes in the North Sea [*Calvès et al.*, 2010; *Davies and Stewart*, 2005; *Stewart*, 2006]. The seismic attributes do not show a con-

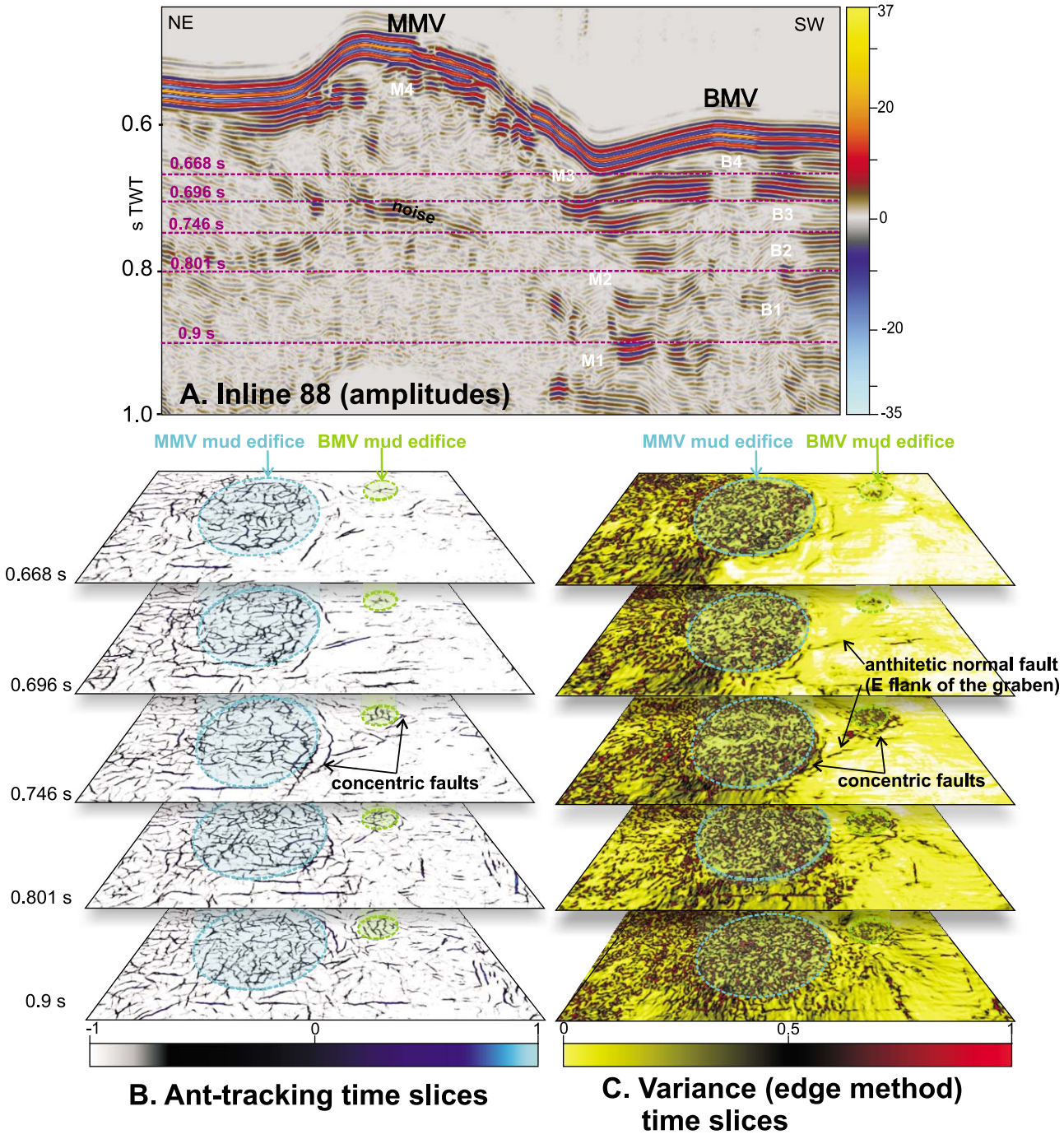

Figure 7. Time slices of different seismic attributes highlighting the internal structure and limits of both mud volcano edifices and its associated concentric faults: (a) inline 88 indicates the time slices with respect to the mud volcano edifices (see location in Figure 2b), (b) ant-tracking time slices, and (c) variance time slices.

centric zonation of the feeder system as proposed by *Roberts et al.* [2010] for mud volcanoes in Azerbaijan. The entire interior of the MMV feeder system is homogenous with the ant-tracking attribute indicating predominantly E-W oriented fractures and some concentric faults at the very edge of the feeder system (Figure 7b), while the structures shown by the variance attribute (Figure 7c) are consistent with tens of meter-sized country rock blocks.

4.2.2. Mudflows and Total Volume of Mud Extruded

[20] We identify a total of four main eruption episodes (M1–M4, from deep to shallow) at the MMV and another four main eruption episodes (B1–B4, from deep to shallow) at the BMV (Figures 6a, 6b, and 8a). In the following we consider these eruption episodes as individual mudflows, but it is possible that some of the episodes consist of several mudflows as indicated by seismic data of even higher resolution

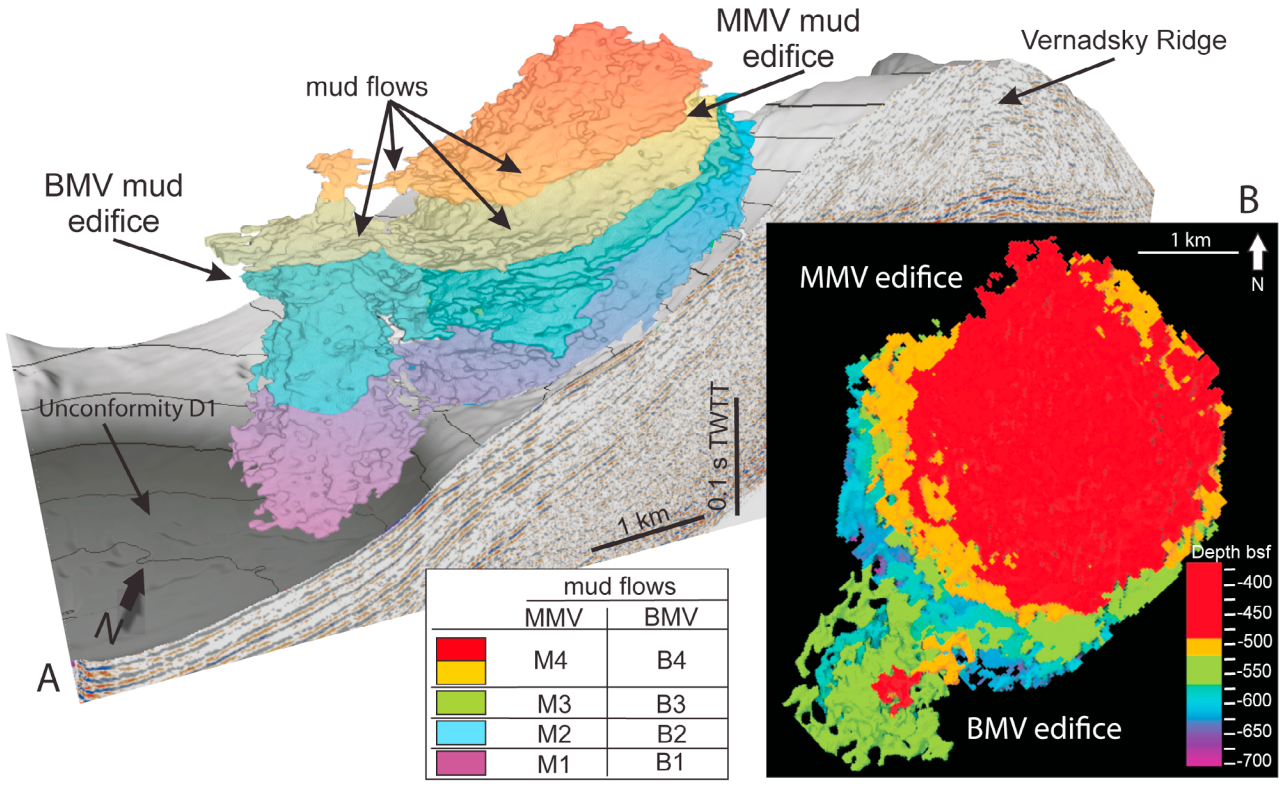

Figure 8. Extracted mud volcano edifices: (a) Mercator mud volcano and buried mud volcano edifices built up from the unconformity D1 (base of mud extrusions) and (b) plan view of both mud edifices, highlighting the overlap of mudflows.

[*Depreiter*, 2009]. The run out distances of mudflows from the MMV (i.e., average distance measured from the geometrical center of the mud volcano to the outer edge of the mudflow) decrease upward from 1900 m to 500 m for mudflows M1–M4. The M1–M4 mudflows extend in a southwestward half spiral from the vertical axis of the MMV (Figure 8a). The run out distances are 400 m, 680 m, 450 m, and 650 m for the mudflows from the BMV (B4–B1, respectively) (Figures 8a and 8b). The three deepest mudflows B1–B3 are almost symmetrically distributed around the vertical axis of the BMV edifice and the shallowest B4 clearly extends eastward toward the MMV (Figure 6b). The deepest mudflows show stacked morphology (M1 and B1) which turns to elongated morphology (M2–M3 and B2–B3) at shallower depths (Figures 6a, 6b, 8a, and 8b). The two youngest mudflows (M4 and B4) again show stacked morphology. Mudflows M1–M3 from MMV and B1–B3 from BMV successively overlap each other (i.e., M1, B1, M2, B2, M3, B3, from deep to shallow), except for the coeval extrusion of the two shallowest mudflows from both mud volcanoes (M4 and B4) (Figure 6a).

[21] The minimum and maximum volumes of mud accumulated from D1 (base unconformity for mud volcano extrusion) to the seabed range between 0.28 and 0.35 km^3 and 0.04–0.05 km^3 for the MMV and the BMV, respectively. Iterative volume extractions over four different seismic attribute workflows show that the degree of uncertainty in the extraction of the final volume of mud from the mud volcanoes is less than 10%, mainly related to the seismic velocity used for the depth conversion.

4.2.3. Geochemistry of Sediment Samples

[22] The surface pore waters in the center of the MMV are highly enriched in Cl and Na: starting from bottom water concentrations that are only slightly higher than normal seawater values, concentrations increase rapidly below the surface and reach more than 5300 mM of Cl at a sediment depth of ~200 cm bsf. In parallel, Na-to-Cl ratios start with the normal seawater ratio of 0.86 at the sediment-water interface and rapidly increase downcore toward a ratio of 1.0. Both the high Cl and Na concentrations as well as the Na/Cl ratio indicate that the pore fluids of the MMV are influenced by halite dissolution at depth. The theoretical halite solubility was calculated for ambient p-T conditions (35 bar, 11°C) to be 6100 mM [*Duan and Li*, 2008; *Greenberg and Møller*, 1989]. In addition, the curvature in the concentration-depth profiles indicates high upward fluid flow velocities. Gas hydrates have not been sampled on Mercator mud volcano. Therefore, it is unlikely that their formation or dissociation has affected the Cl concentrations. Concentrations of dissolved low molecular weight alkanes are elevated in the sediment of the top of the MMV. In combination with the gas emanations, a relatively high methane-to-ethane/propane ratio indicates the presence of highly mature thermogenic gas [*Nuzzo et al.*, 2009], which generally forms at temperatures higher than 120°C.

5. Discussion

5.1. Episodic Eruptions

[23] Correlation of our 3-D seismic data, a 2-D seismic line, and a published seismic line across the El Arraiche

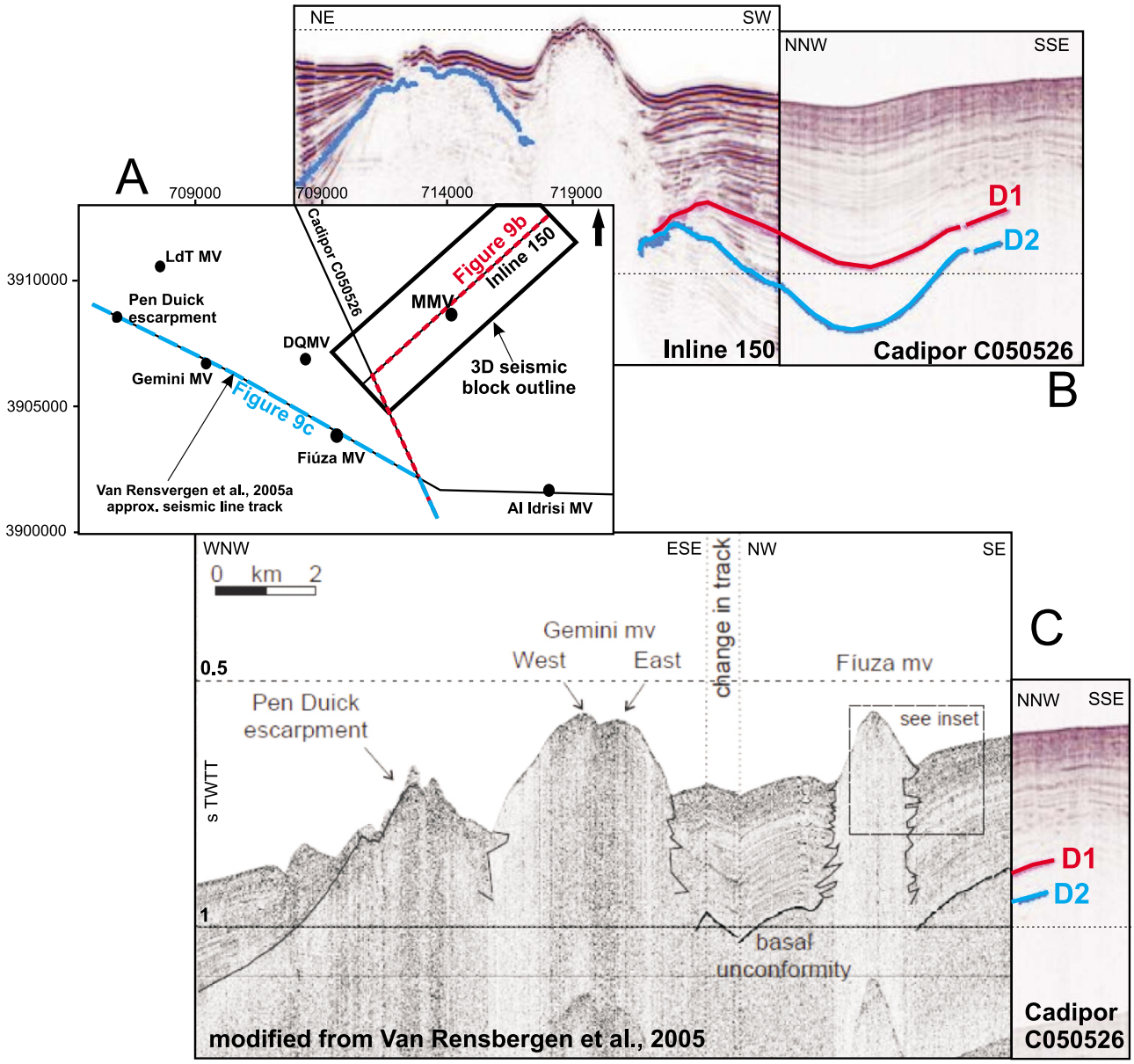

Figure 9. Seismic correlation and relative dating of the base of extrusion: (a) sketch of the locations of seismic lines and mud volcanoes in the El Arraiche field, Lazarillo de Tornes MV (LdT), and Don Quixote MV (DQ); (b) seismic correlation of unconformities D2 and D1 between the 3-D seismic data set (inline 150) and the 2-D line Cadipor050526; and (c) tie between the 2-D line and the unconformities D2 and D1 and a seismic line published by *Van Rensbergen et al.* [2005a, 2005b], showing that their basal unconformity for the mud volcanoes corresponds to unconformity D1.

mud volcanoes [*Van Rensbergen et al.*, 2005a] reveals that the basal unconformity for the mud volcanoes correlates with our unconformity D1 (Figure 9). D1 results from erosion of more than 100 m of sediments in less than 500 kyr during the late Pliocene sea level fall [*Flinch et al.*, 1996; *Hernández-Molina et al.*, 2002]. D2 may result from a previous sea level fall episode, presumably during the late Miocene-early Pliocene, but there is no drilling information to corroborate this. In the following discussion, D2 is only used to discuss dynamic processes of the mud volcano system (MMV and BMV).

[24] During the past 2.6 Myr, eight mud extrusions from MMV (M1–M4) and BMV (B1–B4) stack up as follows: M1, B1, M2, B2, M3, and B3, from deep to shallow. The two youngest mudflows from each mud volcano (M4 and B4) were emplaced at the same stratigraphic depth. Why mud extrusions from the MMV are followed by a mud extrusion from the BMV is not clear. The run-out direction of mudflows from the MMV toward the BMV suggests fast loading (e.g., downward convex curvature at the base of mudflows, Figure 6), which may trigger successive hydrofracturing, mud mobilization and a new extrusion of mud [*Jonk*, 2010].

Table 1. Minimum and Maximum Absolute Values of Extracted Mud Extruded, Mud Discharge Rates, Diameter of Feeder and the Area of Fluid Flow for Both Mercator and Buried Mud Volcanoes[a]

Velocity Time-Depth Conversion[b] (ms^{-1})	Volume of Mud Extruded (km^3)	V (m^3s^{-1})	Diameter of Feeder[c] (m)	Area of Fluid Flow[d] (m^2)
		Mercator Mud Volcano		
1500	0.28	$3.4\ 10^{-6}$	1	3.1
1900	0.35	$4.3\ 10^{-6}$	1.12	3.9
		Buried Mud Volcano		
1500	0.04	$4.9\ 10^{-7}$	0.38	0.45
1900	0.05	$6.1\ 10^{-7}$	0.4	0.5

[a]The modified Stoke's equation [*Kopf and Behrmann*, 2000] is used for diameter calculations. Only valid considering Newtonian fluids and under conditions specified in the text.
[b]Minimum and maximum velocities, respectively.
[c]See equation (1).
[d]Assuming a circular feeder of area = πr^2.

An estimate of the average minimum and maximum flow thicknesses between 45 to 57 m for the MMV and between 30 to 38 m for the BMV mudflows suggests that the thicker mudflows from MMV may overpressure fluids from an earlier BMV mudflow, and may trigger its subsequent activation. Hydrofracturing and mud mobilization may be enhanced by the observed concentric normal faulting on the northwestern side of MMV, which we interpret as caldera-style collapse after eruptions. Such subsidence probably exerts horizontal extensional stress on the BMV, which may open the feeder system. The timing of the individual mudflows suggests that the MMV is above the main feeder of the MMV-BMV mud volcano system, which is also supported by its larger size.

5.2. Mud Discharge Rates and Diameter of the Feeder Conduits

[25] Morphological variations of the mudflows are related to the variation of the fluid content [*Shih*, 1967], sediment properties, and the width of the feeder system [*Kopf and Behrmann*, 2000], i.e., wider feeders correspond to higher discharge rates and elongated morphology [e.g., *Kopf*, 2002; *Kopf and Behrmann*, 2000; *Lance et al.*, 1998; *Van Rensbergen et al.*, 2005b]. In order to calculate the width of the feeder conduits and discuss their relation to the morphology of the mud extrusions, we first divide the calculated volume of mud for both the MMV and the BMV (0.28–0.35 km^3 and 0.04–0.05 km^3, respectively) by the total time span of extrusions (2.6 My). This results in average mud discharge rates (V) that range between 3.4×10^{-6}–4.27×10^{-6} $m^3\ s^{-1}$ and 4.9×10^{-7}–6.1×10^{-7} $m^3\ s^{-1}$ for the MMV and BMV, respectively. We then make the following assumptions to calculate the diameter of feeders for both mud volcanoes:

[26] 1. Mud extrusions from the MMV are formed by clast-bearing mud breccia with a maximum clast radius of r = 0.1 m [*Van Rensbergen et al.*, 2005a], i.e., small compared to the width of the individual feeders.

[27] 2. Mud breccias are formed by clasts of a density of 2600 kg/m^3 [*Robertson and Kopf*, 1998] and by a mud matrix of a wet bulk density of 1600 kg/m^3 [*Kopf and Behrmann*, 2000]. These measurements were made on IODP samples for a similar mud volcano on the Mediterranean Ridge. Both measurements do not include gas, but do include pore water. The range of velocity used for the time-depth conversion of the extracted mud volume constitutes an indicator of gas content within the mud breccias.

[28] 3. The nature of mud extrusions from both MMV and BMV is similar.

[29] 4. Under assumptions 1 and 2, mud breccias in both mud volcanoes behave as a *Newtonian fluid* if their water content exceeds 60% (liquid limit) [*Kopf and Behrmann*, 2000], predicting a viscosity value of 10^6 Pa s. Therefore, we neglect conduit wall friction through the feeder conduit, and viscosity remains constant. In a non-Newtonian scenario, friction and stresses due to the migration of fluids through interstices of the mud edifice (as observed in Figure 7b) may reduce even more the diameter of feeders. Both mud discharge velocities and diameters are in the range of those calculated for the Mediterranean Olimpi and Milano mud volcanoes by *Kopf and Behrmann* [2000].

[30] The modified Stoke's law [*Kopf and Behrmann*, 2000] allows us to calculate the minimum and maximum diameter d for a concentric feeder channel of a width that is cumulative for all the individual feeders:

$$d = \sqrt{\frac{\pi \cdot vol_{mud} \cdot 9\eta}{t \cdot g \cdot \Delta\rho \cdot r^2}} \tag{1}$$

where vol_{mud}/t is the average mud discharge rate V ($m^3\ s^{-1}$), η is the dynamic viscosity (Pa s), g is the acceleration of gravity (9.8 m s^{-2}), $\Delta\rho$ is the effective density of the mud breccia (kg m^{-3}) as the difference between the density of the clast and the density of the clast-bearing matrix ($\Delta\rho = \rho_{clast} - \rho_{matrix}$), and r is the average clast radius (m). This results in minimum accumulated feeder width of 1 m for the MMV and 0.38 m for the BMV (Table 1) with small uncertainties due to seismic velocities that were used for the depth conversion.

[31] By far the largest uncertainty results from using an average discharge rate. The seismic data clearly show the Christmas tree structures for both MMV and BMV indicating that the mud volcanoes were active episodically and not constantly. To investigate the effect of this parameter we vary the discharge rate assuming increasing activity times from 1000 years to 200 000 years, which we consider realistic for the accumulated activity times for the four eruption phases of both mud volcanoes throughout the past 2.6 Myr (Figure 10). The fact that we see individual lobes for one eruption period suggests that the time cannot be much smaller than 250 years for one eruption period and the fact that there is clear onlap onto the mud edifices without small-scale interfingering suggests that the mud volcanoes

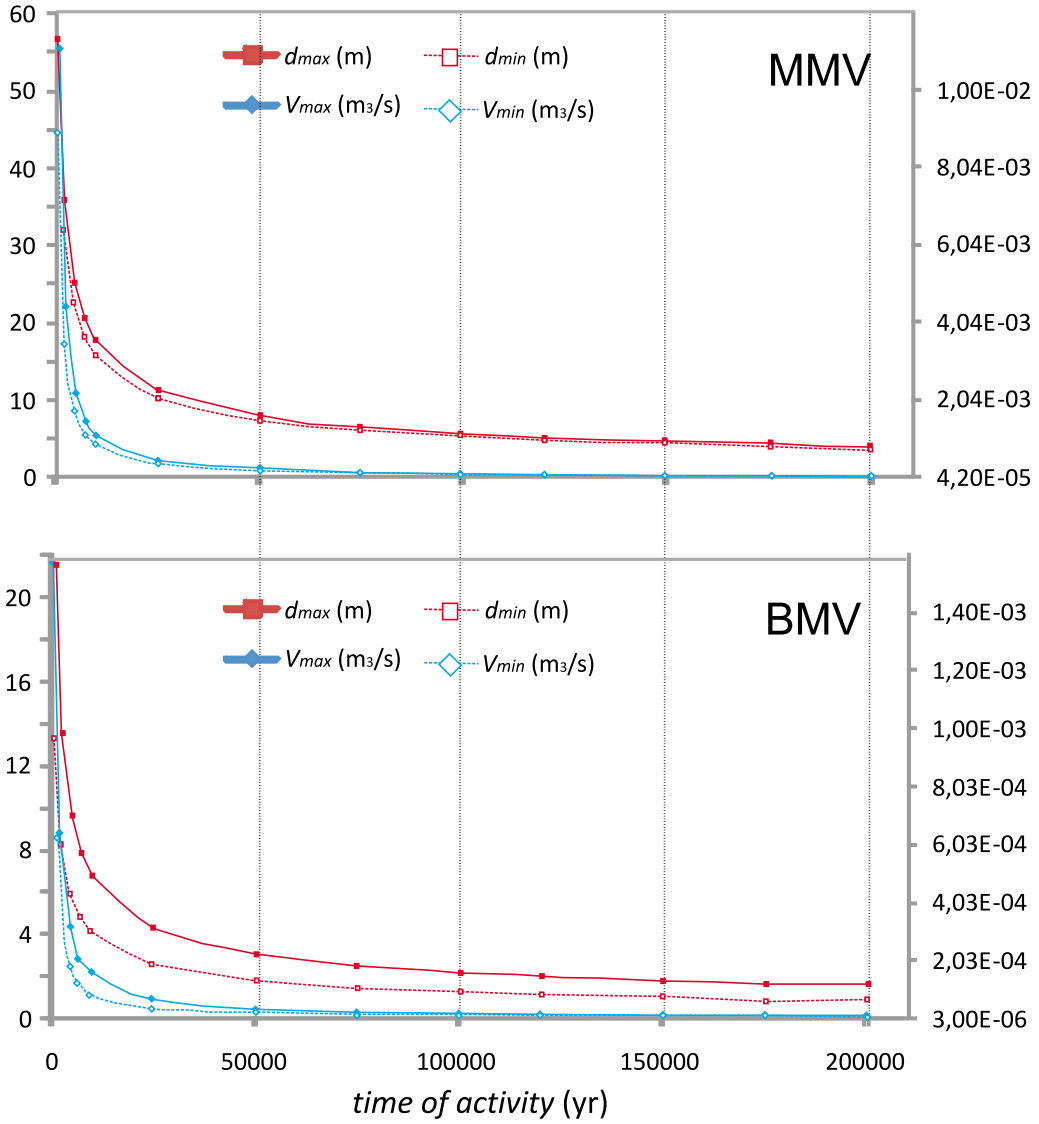

Figure 10. Mud discharge rate V (m^3 s^{-1}) and diameter of feeder conduits d (m) based on the time of activity (yr) of mud volcanoes: (a) maximum and minimum V (blue stacked and dashed lines, respectively) and maximum and minimum d (red stacked and dashed lines, respectively) for MMV; (b) maximum and minimum V (blue stacked and dashed lines, respectively) and maximum and minimum d (red stacked and dashed lines, respectively) for BMV.

are dormant for at least 90% of the time that they exist. Taking this into account for the discharge calculation we obtain a range from 3.17×10^{-6} to 1.59×10^{-3} for the MMV and from 4.4×10^{-5} to 1.1×10^{-2} for the BMV. This translates into cumulative feeder width between 3.6 and 56.6 m for MMV and 1 to 21.4 m for BMV. This agrees with the seismic observations (Figure 7b) that suggest that there are at least ten pathways on a cross section through the MMV, Each pathway must be at least 5 m wide to be detectable in the seismic data. Obviously some of the discontinuities indicated by the ant-tracking attribute may be seismic artifacts and it is not certain that all of the pathways were active at the same time. However, these considerations would suggest that the pathway width for the Mercator Mud Volcano is of the order of 50 m.

[32] Narrower feeders are related to both the progressive degassing as pressure decreases upward to the seafloor and water loss as the mud ascends. The progressive upward loss of viscosity of the mud breccias may result in a stacked morphology of mudflows and, coevally, deeper mudflows will result in an elongate morphology. Following this trend, the progressive upward narrowing of feeders within each mud volcano observed in Figure 7 corresponds to less gas and water in mud breccias and lower mud discharge rates and may explain the morphological change from elongated to stacked mudflows. We propose that the elongate morphology of M2–M3 and B2–B3 is related to wider feeder, higher mud discharge, and higher gas concentration within the mud breccias. The stacked morphology of M4 and B4 is probably related to a later decrease of feeder width, the

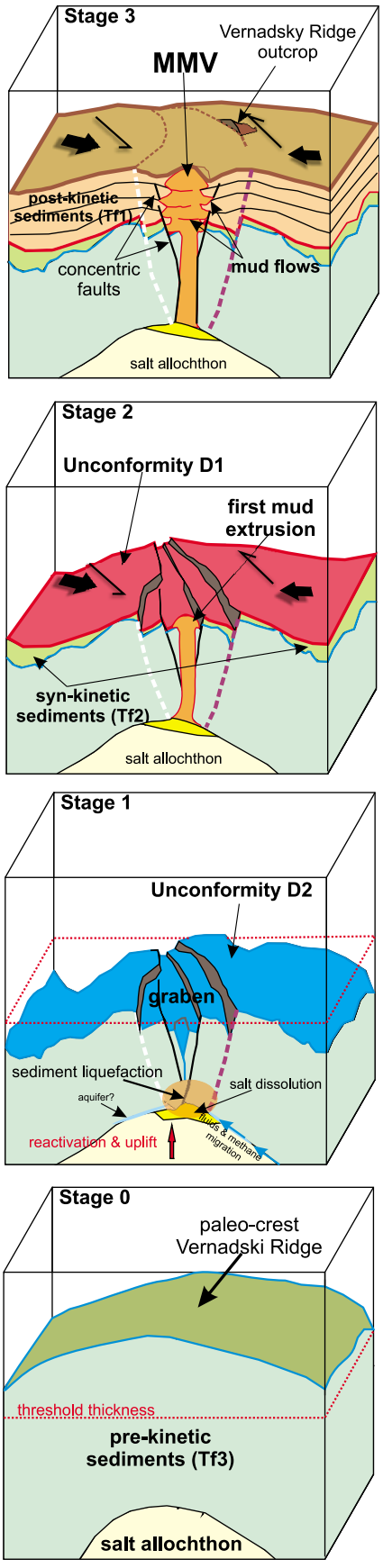

degasification of the mud breccia, and a decrease in mud discharge rate.

5.3. Mud Volcanism in the Presence of Salt

[33] *Hensen et al.* [2007] point out the important role of halokinesis for some mud volcanoes in the Gulf of Cadiz as the upward migrating fluids that result from clay-mineral dehydration at depth show geochemical signatures commonly related to intermediate salt dissolution. The halokinetic control at MMV is suggested by the very high concentrations of Cl and Na, which are close to halite saturation, and a Na/Cl ratio of 1 at only 2 mbsf indicating dissolution of halite. This is strong evidence that MMV is underlain by salt. There are two known possible salt basins affecting the geochemical signature of the MMV: the Moroccan salt basin at 5 km bsf [*Davison*, 2005], located ~30 km westward downslope from the El Arraiche mud volcano cluster (Figure 1) and Triassic salt within the main olistostrome units [*Flinch*, 1993], which do not directly affect the El Arraiche mud volcano field [*Van Rensbergen et al.*, 2005a].

[34] In addition to geochemical results that evidence mid-crustal dissolution at mud volcanoes further north [*Hensen et al.*, 2007], the tectonosedimentary analysis of the 3-D seismic data set suggests that salt has previously moved (i.e., salt allochthon) from the original autochthonous mother salt away from its initial location further west. This uplift formed the Vernadsky Ridge until the shear strength of the overburden equaled the buoyancy forces of the underlying salt, stopping the uplift [*Warren*, 2006]. Erosion at unconformity D2 would have changed the neutral buoyancy conditions of the overburden above the salt allochthon (i.e., Tf3), reactivating the system. Reactive halokinesis typically forms a graben above the salt allochthon [*Warren*, 2006] and as such we interpret the crestal collapse of the Vernadsky Ridge (Figure 4). Later syndeformational sedimentation of Tf2 shows steep onlap on D2 and pinching out of the unit close to the crest of the ridge (Figures 3a and 3c). These are typical indicators of sedimentation affected by salt ascent and crestal subsidence [*Warren*, 2006]. Unconformity D1 (2.6 Ma) truncates the top of Tf2. This suggests increased erosion at the time of ongoing uplift during the late Pliocene sea level fall (D1). Above D1, the flat dipping of internal reflections inTf1 suggests that uplift stopped before deposition of this unit. Minor deformation of TF1 occurred due to renewed subsidence of the graben and concentric faults around the extruded mud edifices (Figures 2a–2d).

[35] We suggest a three-phase evolution of the system in which Tf3, Tf2 and Tf1 correspond to the prekinetic, synkinetic, and postkinetic sedimentation of a reactivated allochthonous salt system, respectively. Although, the very high dissolved Na and Cl concentrations in the pore fluids imply that the fluids must have leached significant amounts of salt in the subsurface, they are not conclusive to the depth at which the salt is presently located. The equilibrium considerations by *Warren* [2006] and the lack of direct evidence for salt within the ~500 m of pene-

Figure 11. Conceptual model relating halokinesis and mud volcanism at the Mercator MV and its dynamics: 0 (initial conditions), 1 (reactivation of halokinesis), 2 (synkinetic mud formation), and 3 (mud volcanism). See text for further explanation.

tration of the seismic data suggest that the bulk of the salt body is at least at 1000 m depth and that the reactivation was triggered by regional-scale erosion.

[36] Previous studies [e.g., *Flinch*, 1993; *Gutscher et al.*, 2009; *Medialdea et al.*, 2004] relate mud volcanism in the Gulf of Cadiz to the Neogene compressive regime associated to sediment liquefaction and mobilization at shallow (0.5–2 km) depths [*Hensen et al.*, 2007]. Due to Neogene compression, deep fluids may migrate upward along the flanks of the intermediate salt allochthon underneath the MMV. Fluids may dissolve the top of the salt allochthon, inducing sediment fluidization and mobilization. Aquifers may also boost the dissolution of the top of the salt allochthon as extra supply of water. The concentric microfaults within and around the edifices of the mud volcanoes (Figure 3b) suggest liquefaction and mobilization of mud just below the penetration of the seismic data at approximately 500 m depth. The coeval ongoing compression of the margin, mineral dewatering and the deposition of Tf1 may have reactivated old conduits during later eruptions. It seems subsequent mud expulsions reoccupied the existing fracture systems, as we do not observe seismic evidence for separate conduits within one feeder system. Although this may be due to insufficient acoustic impedance contrasts between the infill of individual pathways, one would also expect to find buried extinct mud volcanoes at different stratigraphic levels if new pathways were created on a regular basis, but this is not the case. This situation is similar to both the Latakia and Cyprus basins (eastern Mediterranean) where the sources of fluids are located underneath the Messinian evaporites and rise up along faults. Also in those settings fluids dissolve evaporites and mobilize the overburden sediments, which liquefy, fluidize, and extrude as mudflows [*Hübscher et al.*, 2009].

[37] The similar timing of deposition of the extruded mud edifices [*Van Rensbergen et al.*, 2005a] of the mud volcanoes forming the El Arraiche cluster documents their common origin. Although our seismic data set cover just the MMV and the BMV, we suggest that both, near-surface liquefaction and mobilization of mud occurred close to the top of a single salt allochthon underlying both the Renard and the Vernadsky ridges. Mud mobilization was almost certainly enhanced by the presence of free gas advected from depth similar to the other mud volcanoes in the Gulf of Cadiz.

6. Conclusions

[38] We present a model (Figure 11) for the triggering and evolution of the Mercator Mud Volcano closely linked to reactive halokinesis of a salt allochthon at the base of the Vernadsky Ridge. We propose that initially erosion in the late Pliocene reactivated allochtonous salt that was emplaced by nappe tectonics. During the rise of salt, mud formed due to overpressures and mixing with deep fluids. This resulted in periodic mud volcanism since about 2.6 Myr. After the initial uplift, the balance of salt buoyancy and the strength of the overlying sediments were reestablished and the mud volcanism continued episodically and without significant salt movement to the present-day.

[39] Since the late Pliocene, a total of eight mudflows extruded alternately. Each extrusion of mud from the MMV was followed by one from the BMV. We find four main phases of activity for the MMV-BMV system since late Pliocene times. The seismic data show that the total volume of mud extruded (in 2.6 Myr of activity) by the MMV and BMV ranges between 0.28 and 0.35 km^3 and 0.04–0.05 km^3, respectively. The episodic nature of the eruptions and the time interval between the eruptions implies that the much sparser episodes of salt tectonics evidenced by the seismic data are not the only triggering mechanism for mud volcano activity. For ecosystems that depend on methane seepage from the mud volcanoes this implies that they can evolve over long times but that they face episodic extinctions when the mud volcanoes erupt.

[40] **Acknowledgments.** This study has been financed by the EU-HERMES (GOCE-CT-2005-511234-1) project, the German BMBF project COMET (grant 03G0600D), and the NFR project PETROMAKS (169514/530). We thank Ghent University for providing the 2-D seismic data, the captain and the crew of RV *Maria S. Merian*, RRS *Charles Darwin*, and Frode Eriksen of VBPR for their relentless support during the voyage CD178. M.H. would like to thank B. Domeyer, R. Surberg, A. Bleyer, and K. Krieger for assistance with the geochemical work. We are grateful to the Editor, Tom Parsons, Mads Huuse, and an anonymous reviewer who helped to improve the manuscript considerably.

References

Berástegui, X., C. J. Banks, C. Puig, C. Taberner, D. Waltham, and M. Fernández (1998), Lateral diapiric emplacement of Triassic evaporites at the southern margin of the Guadalquivir Basin, Spain, in *Cenozoic Foreland Basins of Western Europe*, edited by A. Mascle et al., *Geol. Soc. Spec. Publ.*, 134, 49–68.

Calvès, G., A. M. Schwab, M. Husse, P. van Rensbergen, P. D. Clift, A. R. Tabrez, and A. Inam (2010), Cenozoic mud volcano activity along the Indus Fan: Offshore Pakistan, *Basin Res.*, *22*, 398–413, doi:10.1111/j.1365-2117.2009.00448.x.

Davies, R. J., and S. A. Stewart (2005), Emplacement of giant mud volcanoes in South Caspian Basin: 3-D seismic reflection imaging of their root zones, *J. Geol. Soc.*, *162*, 1–4, doi:10.1144/0016-764904-082.

Davison, I. (2005), Central Atlantic margin basins of northwest Africa: Geology and hydrocarbon potential (Morocco to Guinea), *J. Afr. Earth Sci.*, *43*, 254–274, doi:10.1016/j.jafrearsci.2005.07.018.

Depreiter, D. (2009), Sources, modes and effects of seabed fluid flow, Ph. D. thesis, Dep. of Mar. Sci., Renard Cent. of Mar. Geol., Ghent Univ., Ghent, Belgium.

Depreiter, D., J. Poort, P. Van Rensbergen, and J. P. Henriet (2005), Geophysical evidence of gas hydrates in shallow submarine mud volcanoes on the Moroccan margin, *J. Geophys. Res.*, *110*, B10103, doi:10.1029/2005JB003622.

Duan, Z., and D. Li (2008), Coupled phase and aqueous species equilibrium of the H_2O– CO_2–NaCl-$CaCO_3$ system from 0 to 250°C, 1 to 1000 bar with NaCl concentrations up to saturation of halite, *Geochim. Cosmochim. Acta*, *72*, 5128–5145, doi:10.1016/j.gca.2008.07.025.

Fernandez-Puga, M. C., J. T. Vazquez, L. Somoza, V. Díaz del Rio, T. Medialdea, M. P. Mata, and R. Leon (2007), Gas-related morphologies and diapirism in the Gulf of Cadiz, *Geo Mar. Lett.*, *27*, 213–221, doi:10.1007/s00367-007-0076-0.

Flinch, J. F. (1993), Tectonic evolution of the Gibraltar Arc, Ph.D. thesis, Rice Univ., Houston, Tex.

Flinch, J., A. W. Bally, and S. Wu (1996), Emplacement of a passive-margin evaporitic allochthon in the Betic Cordillera of Spain, *Geology*, *24*, 67–70, doi:10.1130/0091-7613(1996)024<0067:EOAPME>2.3.CO;2.

Foucher, J.-P., G. K. Westbrook, A. Boetius, S. Ceramicola, S. Dupré, J. Mascle, J. Mienert, O. Pfannkuche, C. Pierre, and D. Praeg (2009), Structure and drivers of cold seep ecosystems, *Oceanography*, *22*(1), 92–109.

Gardner, J. M. (2001), Mud volcanoes revealed and sampled on the Western Moroccan Continental Margin, *Geophys. Res. Lett.*, *28*, 339–342, doi:10.1029/2000GL012141.

Greenberg, J. P., and N. Møller (1989), The prediction of mineral solubilities in natural waters: A chemical equilibrium model for the Na-K-Ca-Cl-SO4–H2O system to high concentration from 0–250°C, *Geochim. Cosmochim. Acta*, *53*, 2503–2518, doi:10.1016/0016-7037(89)90124-5.

Gutscher, M. A., et al. (2009), Tectonic shortening and gravitational spreading in the Gulf of Cadiz accretionary wedge: Observations from multi-beam bathymetry and seismic profiling, *Mar. Pet. Geol.*, *26*, 647–659, doi:10.1016/j.marpetgeo.2007.11.008.

Hensen, C., M. Nuzzo, E. Hornibrook, L. M. Pinheiro, B. Bock, V. H. Magalhaes, and W. Brückmann (2007), Sources of mud volcano fluids

in the Gulf of Cadiz: Indications for hydrothermal imprint, *Geochim. Cosmochim. Acta*, *71*, 1232–1248, doi:10.1016/j.gca.2006.11.022.

Hernández-Molina, F. J., L. Somoza, J. T. Vazquez, F. Lobo, M. C. Fernandez-Puga, E. Llave, and V. Diaz-del Rio (2002), Quaternary stratigraphic stacking patterns on the continental shelves of the southern Iberian Peninsula: Their relationship with global climate and palaeoceanographic changes, *Quat. Int.*, *92*, 5–23, doi:10.1016/S1040-6182(01)00111-2.

Hovland, M., and A. G. Judd (1988), *Seabed Pockmarks and Seepages: Impact on Geology, Biology and the Marine Environment*, 293 pp., Graham Trotman, London.

Hübscher, C., E. Tahchi, I. Klaucke, A. Maillard, and H. Sahling (2009), Salt tectonics and mud volcanism in the Latakia and Cyprus Basins, eastern Mediterranean, *Tectonophysics*, *470*, 173–182, doi:10.1016/j.tecto.2008.08.019.

Jonk, R. (2010), Sand-rich injectites in the context of short-lived and long-lived fluid flow, *Basin Res.*, *22*, 603–621, doi:10.1111/j.1365-2117.2010.00471.x.

Kopf, A. J. (2002), Significance of mud volcanism, *Rev. Geophys.*, *40*(2), 1005, doi:10.1029/2000RG000093.

Kopf, A. J., and J. H. Behrmann (2000), Extrusion dynamics of mud volcanoes on the Mediterranean Ridge accretionary complex, in *Salt, Shale, and Igneous Diapirs In and Around Europe*, edited by B. Vendeville et al., *Geol. Soc. Spec. Publ.*, 174, 169–204.

Lance, S., P. Henry, X. Le Pichon, S. Lallemant, H. Chamley, F. Rostek, J.-C. Faugeres, E. Gonthier, and K. Olu (1998), Submersible study of mud volcanoes seaward of the Barbados accretionary wedge: Sedimentology, structure and rheology, *Mar. Geol.*, *145*, 255–292, doi:10.1016/S0025-3227(97)00117-5.

Maestro, A., L. Somoza, T. Medialdea, C. J. Talbot, A. Lowrie, J. T. Vázquez, and V. Díaz-del-Río (2003), Large-scale slope failure involving Triassic and middle Miocene salt and shale in the Gulf of Cádiz (Atlantic Iberian Margin), *Terra Nova*, *15*, 380–391, doi:10.1046/j.1365-3121.2003.00513.x.

Maldonado, A., L. Somoza, and L. Pallares (1999), The Betic orogen and the Iberian-African boundary in the Gulf of Cadiz: Geological evolution (central North Atlantic), *Mar. Geol.*, *155*, 9–43, doi:10.1016/S0025-3227(98)00139-X.

Mascarelli, A. L. (2009), Quaternary geologists win timescale vote, *Nature*, *459*, 624, doi:10.1038/459624a.

Medialdea, T., R. Vegas, L. Somoza, J. T. Vázquez, A. Maldonado, V. Díaz-del-Río, A. Maestro, D. Córdoba, and M. C. Fernández-Puga (2004), Structure and evolution of the "Olistostrome" complex of the Gibraltar Arc in the Gulf of Cadiz (eastern central Atlantic): Evidence from two long seismic cross-sections, *Mar. Geol.*, *209*, 173–198, doi:10.1016/j.margeo.2004.05.029.

Medialdea, T., L. Somoza, L. M. Pinheiro, M. C. Fernandez-Puga, J. T. Vazquez, R. Leon, M. Ivanov, V. Magalhaes, V. Díaz-del-Río, and R. Vegas (2009), Tectonics and mud volcano development in the Gulf of Cádiz, *Mar. Geol.*, *261*, 48–63, doi:10.1016/j.margeo.2008.10.007.

Nuzzo, M., et al. (2009), Origin of light volatile hydrocarbon gases in mud volcano fluids, Gulf of Cadiz: Evidence for multiple sources and transport mechanisms in active sedimentary wedges, *Chem. Geol.*, *266*, 350–363, doi:10.1016/j.chemgeo.2009.06.023.

Pedersen, S. I., T. Skov, T. Randen, and L. Sønneland (2005), Automatic fault extraction using artificial ants, *Math. Ind.*, *7*, 107–116, doi:10.1007/3-540-26493-0_5.

Pedersen, S. I., T. Randen, L. Sønneland, and O. Steen (2002), Automatic 3-D fault interpretation by artificial ants, paper presented at 64th EAGE Conference and Exhibition (G037), Eur. Assoc. of Geosci. Eng., Florence, Italy.

Petersen, C. J., S. Bünz, S. Hustoft, J. Mienert, and D. Klaeschen (2010), High-resolution P cable 3-D seismic imaging of gas chimney structures in gas hydrated sediments of an Arctic sediment drift, *Mar. Pet. Geol.*, *27*, 1981–1994, doi:10.1016/j.marpetgeo.2010.06.006.

Pinheiro, L. M., et al. (2003), Mud volcanism in the Gulf of Cadiz: Results from the TTR-10 cruise, *Mar. Geol.*, *195*, 131–151, doi:10.1016/S0025-3227(02)00685-0.

Planke, S., and C. Berndt (2002), Anordning for seismikkmåling, Patent 317651, Norwegian Industrial Property Office, Oslo.

Roberts, K. S., R. J. Davies, and S. A. Stewart (2010), Structure of exhumed mud volcano feeder complexes, Azerbaijan, *Basin Res.*, *22*, 439–451, doi:10.1111/j.1365-2117.2009.00441.x.

Robertson, A. H. F., and A. Kopf (1998), Tectonic setting and processes of mud volcanism on the Mediterranean ridge accretionary complex: Evidence from Leg 160, in *Proceedings of the Ocean Drilling Program, Scientific Results*, vol. 160, edited by A.H.F. Robertson et al., pp. 665–680, Ocean Drill. Program, College Station, Tex.

Rosenbaum, G., G. S. Lister, and C. Duboz (2002), Relative motions of Africa, Iberia and Europe during Alpine orogeny, *Tectonophysics*, *359*, 117–129.

Sandwell, D. T., and W. H. F. Smith (1997), Marine gravity anomaly from Geosat and ERS 1 satellite altimetry, *J. Geophys. Res.*, *102*, 10,039–10,054, doi:10.1029/96JB03223.

Scholz, F., C. Hensen, A. Reitz, R. L. Romer, V. Liebetrau, A. Meixner, S. M. Weise, and M. Haeckel (2009), Isotopic evidence ($^{87}Sr/^{86}Sr$, δ^7Li) for alteration of the oceanic crust at deep-rooted mud volcanoes in the Gulf of Cadiz, NE Atlantic Ocean, *Geochim. Cosmochim. Acta*, *73*, 5444–5459, doi:10.1016/j.gca.2009.06.004.

Shih, T. A. (1967), A survey of the active mud volcanoes in Taiwan and a study of their types and the character of the mud, *Pet. Geol. Taiwan*, *5*, 259–311.

Somoza, L., A. Maestro, and A. Lowrie (1999), Allochthonous blocks as hydrocarbon traps in the Gulf of Cadiz, paper presented at the Offshore Technology Conference, pp. 571–577, Am. Assoc. Pet. Geol., Houston, Texas, doi:10.4043/10889-MS.

Somoza, L., et al. (2003), Seabed morphology and hydrocarbon seepage in the Gulf of Cadiz mud volcano area: Acoustic imagery, multibeam and ultra-high-resolution seismic data, *Mar. Geol.*, *195*, 153–176, doi:10.1016/S0025-3227(02)00686-2.

Stewart, S. A. (2006), Implications of passive salt diapir kinematics for reservoir segmentation by radial and concentric faults, *Mar. Pet. Geol.*, *23*, 843–853, doi:10.1016/j.marpetgeo.2006.04.001.

Tari, G., J. Molnar, P. Ashton, and R. Hedley (2000), Salt tectonics in the Atlantic margin of Morocco, *Lead. Edge*, *19*, 1074–1078, doi:10.1190/1.1438481.

Van Bemmel, P., and R.E.F. Pepper (2000), Seismic signal processing method and apparatus for generation a cube of variance values, Patent number 6151555, U.S. Patent and Trademark Off., Washington, D. C.

Van Rensbergen, P., D. Depreiter, M. K. Ivanov, and the Shipboard Scientific Party (2003), El Arraiche mud volcano field, in *Interdisciplinary Geoscience Research on the Northeast Atlantic Margin, Mediterranean Sea and Mid-Atlantic Ridge*, edited by N. H. Kenyon et al., *IOC Tech. Rep. Ser.*, 67, pp. 43–51, U.N. Educ. Sci. and Cult. Off., Paris.

Van Rensbergen, P., et al. (2005a), The El Arraiche mud volcano field at the Moroccan Atlantic slope, Gulf of Cadiz, *Mar. Geol.*, *219*, 1–17, doi:10.1016/j.margeo.2005.04.007.

Van Rensbergen, P., D. Depreiter, B. Pannemans, and J. P. Henriet (2005b), Seafloor expression of sediment extrusion and intrusion at the El Arraiche mud volcano field, Gulf of Cadiz, *J. Geophys. Res.*, *110*, F02010, doi:10.1029/2004JF000165.

Vázquez, J. T., and R. Vegas (2000), Different styles of deformation in the Africa-Eurasia plate boundary, from the Horseshoe arc to the Alboran sea, paper presented at 2nd Asamblea Hispano-Portuguesa de Geodesia y Geofisica, (S03–19), Inst. Geogr. Nac., Lagos, Portugal.

Warren, J. K. (2006), *Evaporites: Sediments, Resources and Hydrocarbons*, Springer, Berlin, doi:10.1007/3-540-32344-9.

Wessel, P., and W. H. F. Smith (1998), New, improved version of the Generic Mapping Tools Released, *Eos Trans. AGU*, *79*, 579, doi:10.1029/98EO00426.

C. Berndt, M. Haeckel, L. Haffert, and D. Klaeschen, IFM-GEOMAR, Leibniz Institute of Marine Sciences, Kiel University, Wischhofstr. 1-3, D-241248 Kiel, Germany.

D. Depreiter, Renard Centre of Marine Geology, Department of Geology and Soil Science, Ghent University, 9000 Gent, Belgium.

J. Mienert and C. Perez-Garcia, Department of Geology, University of Tromsø, Dramsveien 201, N-9037 Tromsø, Norway. (carolina.garcia@ig.uit.no)